

Apparatus for the Measurement of Electromagnetic Activity of Landslides

Krzysztof Maniak^{1*}, Remigiusz Mydlikowski²

¹ National Institute of Telecommunications, ul. Szachowa 1, 04-894 Warsaw, Poland

² Faculty of Electronics, Photonics and Microsystems, Wrocław University of Science and Technology, ul. Janiszewskiego 11/17, 50-372 Wrocław, Poland

* Corresponding author's e-mail: k.maniak@il-pib.pl

ABSTRACT

The article presents a new research apparatus for measuring the electromagnetic activity of landslides. The basic element of the apparatus is a highly sensitive underground receiver of the magnetic component of the EM field. Such a receiver inserted to the full depth of a landslide well records the levels of magnetic field amplitude at a given depth. Anomalous levels of the magnetic component indicate the existence of landslide slip planes. Combining several receivers into a measurement system will enable continuous monitoring of landslide activity. The article presents examples of studies using the discussed apparatus, which were carried out on real landslides.

Keywords: landslide, electromagnetic emission, movement prediction

INTRODUCTION

Landslides, like earthquakes, volcanic eruptions or hurricanes, pose a serious threat to human life and health and the safety of residential or industrial infrastructure [1]. Despite increasingly advanced research into the mechanism of landslide activity resulting in the development of better methods for their stabilization [2] and early warning of possible landslide activity, newer and more effective methods are being sought to predict and monitor their movements. It is important here to know the geological structure of the landslide with the distinction of slip zones in which the displacement of landslide layers occurs. Due to the occurring landslide processes, different types of landslides are distinguished [3]. In simple terms, in the slip zone there is a slip plane, where the movement of landslide masses occurs under the influence of the sliding force. It is observed that landslide activity is associated with long-term meteorological events, such as rainfall [4]. The traditional method used for years to track

landslide movements is the inclinometer method [5, 6]. However, most methods monitor the landslide process in discrete moments of time or give information about the movement of a landslide when catastrophic movement begins. According to many researchers, it is valuable to have information about the immediate increase in the sliding force near the slip plane before the landslide movement even occurs [7]. A significant portion of mechanical energy is released in this zone. Landslide studies use surface survey methods and those that require interference with the internal structure of the landslide body. For example, external monitoring of the movement of the landslide body can be carried out with great precision, through the use of GPS (Global Positioning System) apparatus [8, 9]. A GIS (Geographic Information System) method is used to predict the movement of more extensive landslide areas [10]. Traditional geoelectric methods, such as mapping the resistivity of the landslide body, are also used. The surveys look for areas with relatively low resistivity, which is associated with increased

water accumulation, promoting the development of landslide movements [11]. Commonly used in landslide monitoring is the eigenpotential method [12]. The eigenpotential method is often used in conjunction with monitoring the resistivity of the landslide body [13]. Of great importance in obtaining information about the structure of the landslide under study are measurements made with GPR (Ground Penetrating Radar) [14]. Significant landslide areas are monitored with the participation of satellites [15]. To predict the development of landslide movements also uses advanced modelling using neural networks and machine learning algorithms [16, 17]. Similar solutions are used for earthquake forecasting [18]. However, methods are constantly being sought for continuous tracking of landslide processes, capable of alerting the relevant services before catastrophic development of landslide processes occurs. The method presented by the authors of this paper is part of this trend. This method is based on the measurement of electromagnetic radiation emitted by an active landslide. Elevated EM emissions occur in landslide-active zones and are measurable before the catastrophic development of the landslide process. The proposed apparatus is equipped with an underground measuring receiver sensitized to the magnetic field. The size of the receiver is small and it is possible to insert it into existing boreholes drilled for inclinometric landslide research. The research methods used so far are based on measurements of electromagnetic fields emitted during landslide activity using mainly ground-based antennas [19, 20, 21]. Measurement apparatuses are characterized by a significant degree of complexity to eliminate ground-based interference signals from human infrastructure. An additional problem is their low sensitivity and the inability to indicate the inundation of the slip plane. The results obtained may be subject to considerable measurement errors. This fact argues for the use of a small-sized underground measuring probe inserted into the body of the landslide for the study. Such a probe can be located near the slip zone of the landslide.

EM RADIATION GENERATION MECHANISMS

Piezoelectric effect

In the body of an active landslide, within the slip plane, there are stresses with significant

values acting on the material from which the landslide is built. There is a wide group of materials forming geological structures, including landslides, that exhibit piezoelectric properties. Naturally occurring piezoelectric minerals include quartz, tourmaline, sphalerite, nepheline [22]. The piezoelectric effect is also observed in minerals with dielectric and semiconducting properties, such as selenium, tellurium, greenockite, zincite, kdmoseelite. The relation describing the piezoelectric effect takes the form [22]:

$$\vec{D} = \varepsilon\vec{E} + d\vec{T} \quad (1)$$

where: \vec{D} – electric displacement [C/m²],

\vec{T} – stress [N/m²],

\vec{E} – electric field [V/m],

ε – electrical permeability [F/m],

d – piezoelectric constant [C/N].

From the quoted relationship, it follows that under the influence of the stress forced in the sample, there is a proportional change in the electrical induction, also referred to as electric shift. This phenomenon is commonly referred to in the literature as reverse piezoelectric phenomenon.

Electric double layer

The fluid-saturated geological layers that form a landslide can be considered at the microscale as a network of capillaries formed in the granular structure of the medium. In the fluid filling the capillaries, ions are raised, which interact with the grains of the medium to form an electrical double layer, as shown in Figure 1 using the Stern model [23].

According to Figure 1a, the layer of cations located in the Stern layer, immediately adjacent to the capillary wall with a surface potential of φ_0 , is deprived of the ability to move in solution as a result of strong electrostatic attraction and van der Waals forces [24]. Cations in the diffusion layer have the ability to move in solution, but their concentration is increased as a result of electrostatic interactions. The plane separating the layer of stationary ions and the diffusion layer is called the slip plane. It has a well-defined potential, called ζ -potential or electrokinetic potential. The value of the potential ζ strongly depends on the type of medium saturated with the liquid, as well as the properties of the liquid itself, which in most cases can be treated as an electrolyte. For example, for kaolinite, the average value of ζ -potential is 10–50 mV.

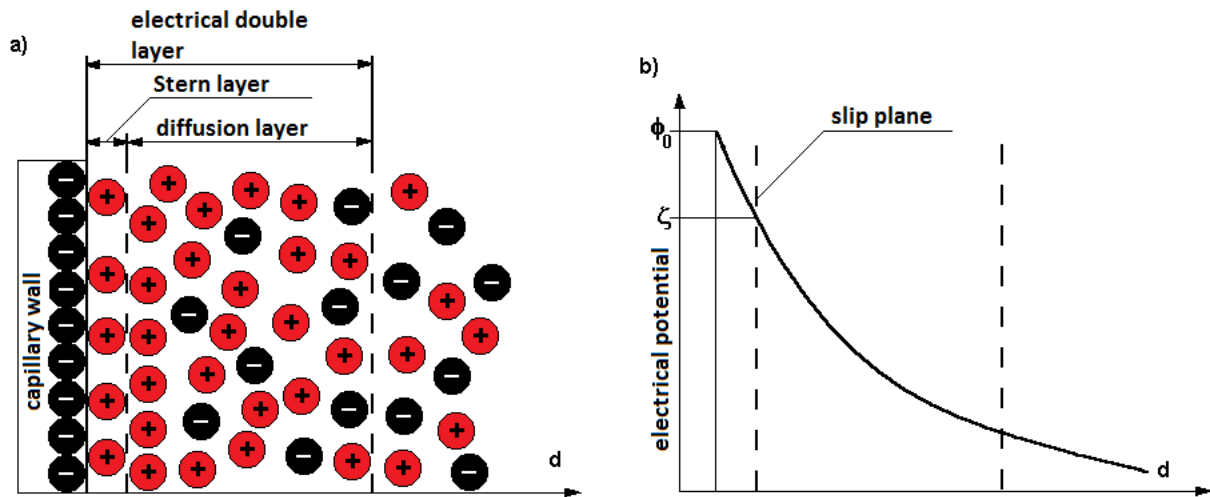


Fig. 1. Stern model of an electrical double layer: a) ion distribution near the capillary wall b) potential distribution as a function of distance from the capillary wall [23]

The Stern layer together with the diffusion layer form the EDL electrical double layer. The course of the electric potential as a function of distance from the capillary wall is shown in Figure 1b.

Relationships linking fluid flow in a homogeneous porous medium with phenomena of electrical nature take the form [25, 26, 27]:

$$\vec{J}_V = L_{11}\nabla(-p) + L_{12}\nabla(-V) \quad (2)$$

$$\vec{J}_C = L_{21}\nabla(-p) + L_{22}\nabla(-V) \quad (3)$$

where: \vec{J}_V – density of the liquid stream [m/s],
 \vec{J}_C – current density [A/m²],
 p – pressure of the liquid stream [N/m²],
 V – electric potential [V],
 $L_{11}, L_{12}, L_{21}, L_{22}$ – proportionality coefficients.

Considering a theoretical sample of the pore medium in the shape of a cylinder with a base area A and length l , through which liquid flow is forced in the direction of length l , under the influence of a pressure difference Δp . The pore structure of a cylinder with resultant resistivity ρ_p is saturated with a liquid with resistivity ρ_c . From this, the voltage U_p occurring at the ends of the sample can be determined [23].

$$U_p = \frac{\varepsilon \zeta \rho_c}{\eta} \Delta p \quad (4)$$

where: η – dynamic viscosity of the liquid [N·s/m²]

The resistance R_p of the pore structure of the sample is:

$$R_p = \frac{\rho_p l}{A} \quad (5)$$

The current I_p flowing through the sample can be determined by the relation [28]:

$$I_p = \frac{\varepsilon \zeta \rho_c}{\eta \rho_p} A \frac{\Delta p}{l} \quad (6)$$

where: $\Pi = \rho_c / \rho_p$ – dynamic porosity coefficient [28].

Treating a cylindrical sample with base radius r as a rectilinear conductor through which a current of I_p flows, according to Biot-Savart's law, the magnetic field strength can be determined at an observation point d away from the sample ($d \gg r$):

$$\vec{H}_P = \frac{I_p}{\pi} \int \frac{d\vec{l} \times \vec{d}}{d^3} \quad (7)$$

Taking into account relation (6) and assuming the observation point normal to the side of the cylinder, we get:

$$\vec{H}_P = \frac{l I_p}{4\pi d^2} \hat{d} \quad (8)$$

The emission of variable electromagnetic fields caused by fluid flow is due to the fact of oscillatory or pulsed changes in the pressure gradient forcing the flow [29, 30].

Microcracks

In the body of the landslide in the vicinity of the slip plane there is considerable mechanical stress on the matter. In the fractions adjacent to the slip plane, a network of microcracks is formed [2]. This phenomenon leads to the release of energy in the form of EM field emissions. The microcrack propagates in the landslide matter and its walls perform mechanical vibrations. This situation is shown in Figure 2.

Charges of opposite signs accumulate on opposite walls of the microcrack, which are distant by w . Their distance oscillates around the distance w becoming the source of EM field emission. The relation describing the magnitude of magnetic field induced by the microcrack takes the form [31]:

$$H = \frac{I_0 w}{4\pi r} \sin\theta \cdot \arctan\left(\frac{c}{r}\right) i \quad (9)$$

This signal can be recorded by the measuring receiver.

LABORATORY MEASUREMENT SYSTEM

A series of preliminary laboratory tests were carried out before designing the apparatus for monitoring the values of electromagnetic field emissions from landslides. It was evaluated what frequencies and values of electromagnetic field intensities are emitted by samples of rocks and soils that can form a fraction of real landslides. For this purpose, a laboratory station was set up as in Figure 3.

The essence of the tests consists in exerting axial loads on the test specimen through a hydraulic press. The jaws of the press between which the sample is placed are shielded by an electromagnetic shield to protect against parasitic electromagnetic disturbances.

Tests on the created stand can be carried out in three different ways:

- *Crushing of rock samples in the form of finished blocks.* Sample placed between the jaws of the press subjected to an axial force. Measurement of electromagnetic emission by internal electric field receivers E and magnetic field receivers H.
- *Crushing of loose materials.* Bulk material (gravel, sand) filling a special cylinder with a piston, subjected to the force of the press jaws. Measurement of EM emissions by E and H receivers.
- *Measurement of electrical potentials emitted by plastic materials.* Measuring electrodes (Electrodes) were attached to the jaws of the press to measure the potentials present on the crushed sample of plastic material (e.g. clay).

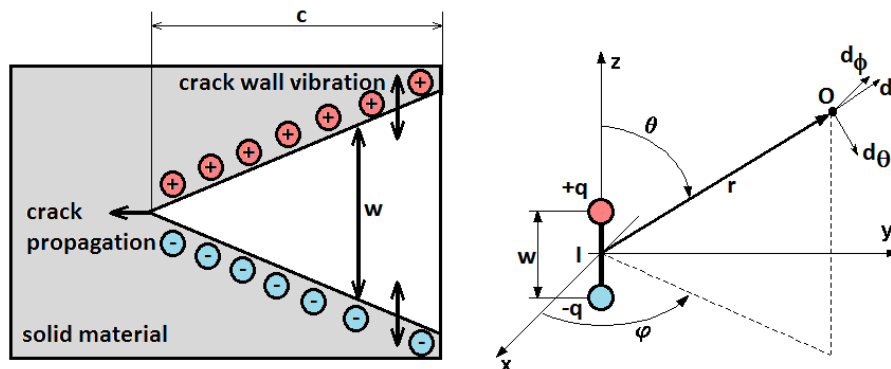


Fig. 2. The nature of EM field generation through microcracks

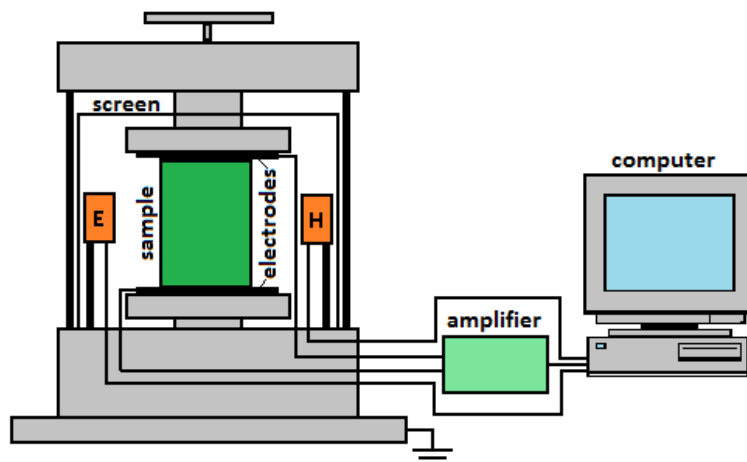


Fig. 3. Laboratory station for testing electromagnetic field emissions from material samples

Laboratory test results

Figure 4 shows the results of measuring the difference in electrical potential recorded by Electrodes during the exertion of an increasing pressure force on a clay sample.

Figure 5 presents the emission waveform of the magnetic component of the EM field along with the frequency spectrum for an example sandstone rock sample in the form of a uniform block. Figure 6 presents the results obtained from crushing gravel in a piston measuring cylinder.

The electric components of the EM field recorded in the latter two cases showed a similar character to the magnetic component. Due to the greater susceptibility of these signals to external interference, they were omitted from the publication. Based on the research performed, the following observations were made:

- Exerting a linearly increasing compressive pressure on the clay sample resulted in

a voltage recorded by Electrodes. The value of this voltage increased in proportion to the force of the pressure.

- When a sandstone block is destroyed, a strong single pulse of magnetic field emission occurs at the time of its disintegration. The maximum amplitude values of the frequency spectrum striations, obtained during the measurements, reached levels of up to $1.5 \cdot 10^{-3}$ A/m.
- By crushing a sample of gravel placed in the measuring cylinder, a series of consecutive EM pulses corresponding to the destruction of the gravel particles were observed. The recorded maximum values of the spectrum bars were at up to $2 \cdot 10^{-5}$ A/m.
- For the sandstone sample, the useful spectrum of emitted signals extends to a value of 10 kHz
- In the case of the gravel sample, the useful spectrum is contained up to a value of 20 kHz, taking its maximum near the frequency of 16 kHz.

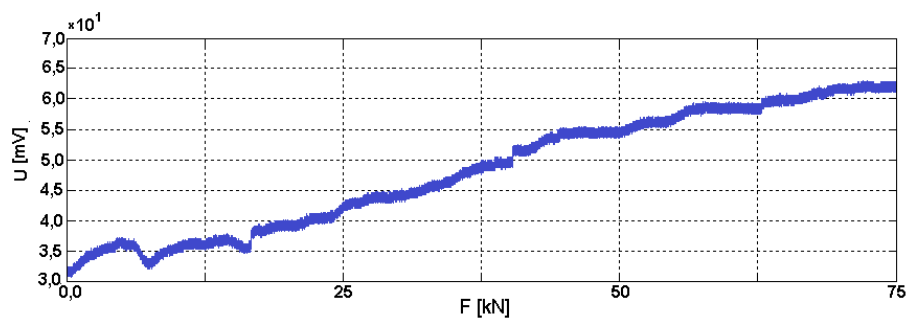


Fig. 4. Variation of the potential difference at the extremities of the clay sample as a function of contact force

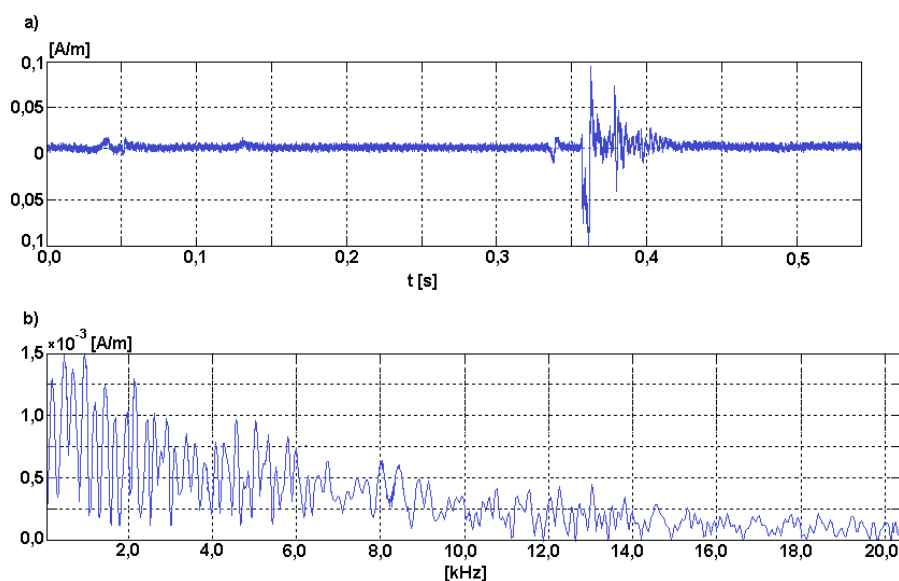


Fig. 5. Emission of magnetic component of electromagnetic field during destruction of sandstone sample: a) time course b) frequency spectrum

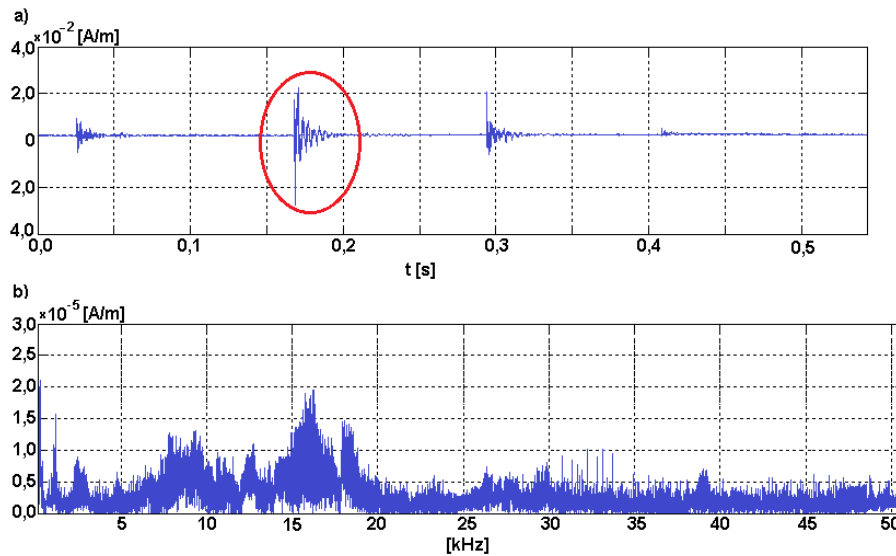


Fig. 6. Emission of the magnetic component of the electromagnetic field during loading of the gravel sample: a) time course b) frequency spectrum for the marked pulse

MEASUREMENT SYSTEM DESIGN

Based on the results of laboratory measurements and with a view to the practical implementation of the measurement system, a solution was developed, the block diagram of which is shown in Figure 7. The measurement system consists of an underground magnetic field receiver, which during the measurements is inserted into a borehole drilled in the body of the landslide. The receiver with the ground part of the measurement system (processing block) is connected by a fiber optic line. The advantage of the fiber optic cable used is the lack of sensitivity to parasitic signals of electromagnetic disturbances. Precise guidance of the receiver in the borehole, along with the measurement of the depth at which it was inserted, is provided by a rotary drum on which 50m of kevlar fiber-reinforced optical fiber is wound.

The underground magnetic field receiver, which was guided along the underground borehole, was placed in a hermetic casing with a size of $\phi 40 \times 500$ mm. The measuring antenna of the receiver was made on a ferrite rod with a diameter of 20mm and a length of 100mm and a number of coils of 1000 turns. Due to the expected low values of recorded magnetic field intensities (of the order of a minimum of 10^{-5} A/m), EM-emitting digital blocks were abandoned in the construction of the receiver. The schematic diagram of the magnetic field receiver is shown in Figure 8, while Figure 9 shows a view of the interior of the magnetic field receiver.

In the diagram (Fig. 8), a parallel resonant circuit consisting of antenna coil L and switched capacitances C1-C3 is sensitized to the presence of the magnetic component of the EM field. Depending on the selected capacitance, the circuit manifests its maximum sensitivity at frequencies of 7,

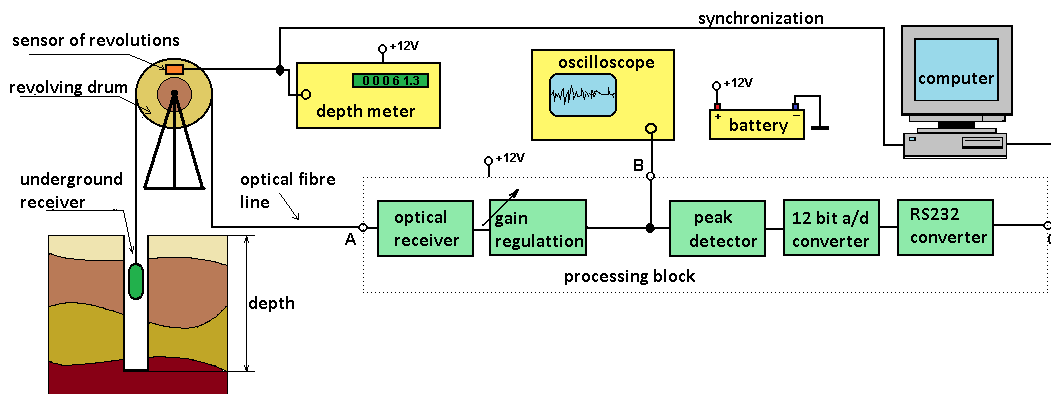


Fig. 7. Block construction of a system for measuring EM activity of landslides

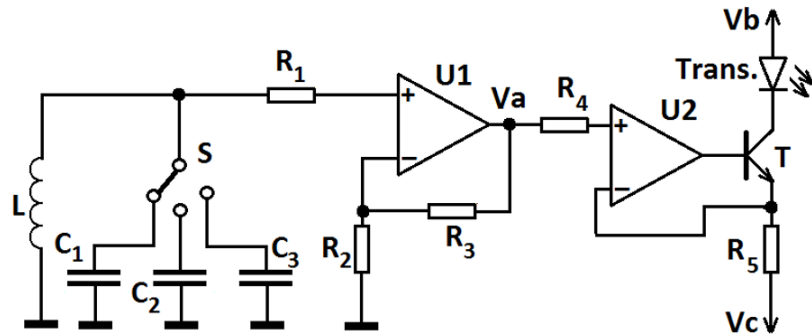


Fig. 8. Schematic diagram of underground magnetic field receiver

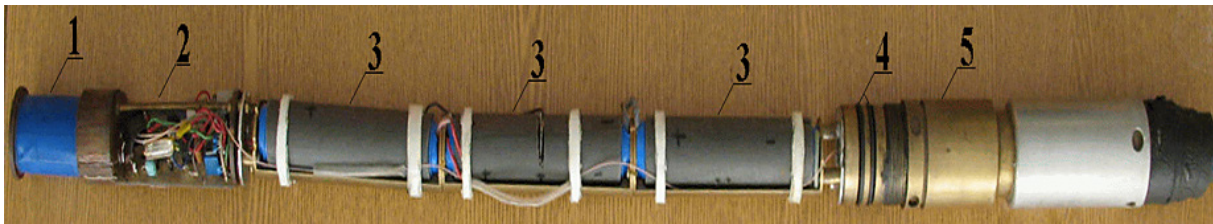


Fig. 9. Interior view of the underground magnetic field receiver: 1 – ferrite antenna; 2 – electronic system; 3 – Li-Ion battery assembly; 4 – O-rings; 5 – probe support structure

14 and 19 kHz. These frequencies were chosen as representative of the characteristics of the spectra recorded during laboratory measurements.

The value of the selected L and C elements of the system for a given measurement frequency, is related by the relation [32]:

$$f = \frac{1}{2 \cdot \pi \sqrt{L \cdot C}} \quad (10)$$

where: L – inductance of antenna coil [H],
 C – capacity [F].

The induced value of the electromotive force (EFA) in the antenna circuit is [33]:

$$EF_A = h_{ef} \cdot E \cdot \psi(\alpha) \quad (11)$$

where: h_{ef} – height (effective height) of the antenna [m],
 E – electric field strength [V/m],
 $\psi(\alpha)$ – coefficient of the dependence of the induced EF on the position of the antenna with respect to the field lines.

At the terminals of the antenna, for a given measurement frequency, we have a voltage [33]:

$$U = Q \cdot EF_A = Q \cdot h_{ef} \cdot E \cdot \psi(\alpha) \quad (12)$$

where: Q – goodness of the resonant circuit.

Under free space conditions, the relationship [34] becomes true:

$$E = Z_0 \cdot H = 120\pi \cdot H \quad (13)$$

where: H – magnetic field strength [A/m]

$Z_0 = 120\pi$ [Ω] – wave impedance of free space.

Using relation (13) in formula (12) we get:

$$U = 120\pi \cdot Q \cdot h_{ef} \cdot H \cdot \psi(\alpha) \quad (14)$$

The receiver uses a closed magnetic antenna with a ferrite core. For an antenna of this type, the effective height h_{ef} [34] is:

$$h_{ef} = \frac{2\pi z S \mu \cos\alpha}{\lambda} \quad (15)$$

where: z – number of antenna coils,
 S – area covered by the antenna coil [m²],
 λ – wavelength [m],
 μ – magnetic permeability effective core of ferrite antenna [H/m],
 α – angle formed by the plane of the coil with the direction of propagation of the electromagnetic wave.

At the same time, the relationship [34] is valid:

$$h_{ef} = \frac{EF_A}{E} \quad (16)$$

where: EF_A – electromotive force induced in the antenna [V],
 E – electric field strength [V/m].

Finally, after taking into account the relationship (13) can be written:

$$EF_A = Z_0 \cdot H \cdot h_{ef} = \frac{240\pi^2 z S \mu}{\lambda} H \cdot \cos\alpha \quad (17)$$

In view of the above, the voltage at the terminals of a parallel resonant circuit of an antenna of Q goodness under resonant conditions is:

$$U = Q \cdot E_A = \frac{240\pi^2 z S \mu}{\lambda} H \cdot Q \cdot \cos \alpha \quad (18)$$

The voltage obtained in the resonant circuit is fed to the amplifier realized on the operational amplifier U1, the gain of which is expressed by the relation [32]:

$$G = 1 + \frac{R_3}{R_2} \quad (19)$$

The fixed gain of the block is 10V/V. Further amplification of the signal takes place in the ground-based signal processing block acquired from the fiber optic receiver. The last module in the signal processing block is the optical fiber transmitter, which is controlled by a voltage-controlled current source. The source is composed of an operational amplifier U2, a transistor T and a resistance R_5 . The forced current in the optical transmitter diode is determined by the relation [32]:

$$I = \frac{V_a - V_c}{R_5} \quad (20)$$

Processing of the signal sent by the receiver to the ground surface is provided by the processing block, the simplified schematic diagram of which is presented in Figure 10. The optical signal fed to the input A is converted into an electrical signal using a specialized HFBR 2416 element from Avago. Elements U1, R1, C1 and C2 provide power to the element with the appropriate 5V stabilized voltage. Capacitance C3 cuts off the DC component against which the actual measurement signal occurs. Then the measured signal is fed to the member made on the operational amplifier U2, which allows adjustable gain in the range

of 10–100 V/V by means of a potentiometer P provided with an appropriate scale. At this point, it is possible to control the received signal, for example, using an oscilloscope at the electrical output B. In the next part, the tested signal is subjected to peak detection in a circuit consisting of elements U3, R4 and D. Further, the voltage value corresponding to the peak value of the signal is converted into digital form and, after conversion to the RS232 standard, it is possible to record in computer memory. Recording takes place at discrete moments of the receiver's immersion in the structure under study, which is provided by a depth meter circuit that sends an appropriate synchronizing pulse. Recording takes place every 5cm of the receiver's immersion in the measuring hole. The circuit made on the U4 amplifier provides symmetrization of the power supply voltage obtained from the 12V battery supplying the entire ground system.

MAGNETIC FIELD MEASUREMENTS ON REAL LANDSLIDES

The discussed measuring system for studying spontaneous magnetic field emission, was used to study the stability of real landslides. The article presents sample results from a periodically inactive landslide in Szymbark near Gorlice (Poland) and an active landslide in Jaroszw near Strzegom (Poland).

A periodically inactive landslide in Szymbark

A study of the magnetic component emission of the field at the landslide in Szymbark was

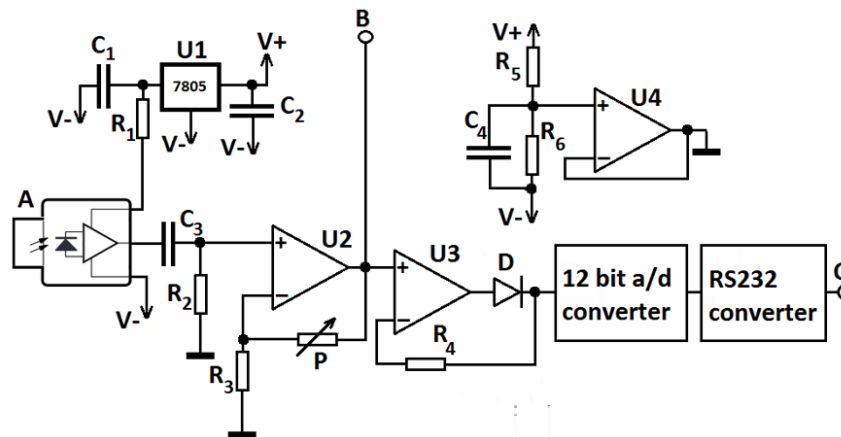


Fig. 10. Electrical schematic of the signal processing block of the system for measuring the electromagnetic activity of landslides

conducted. The studied landslide is developed in homogeneous deposits of clay mixed with sand. The bedrock of the landslide, lying at a depth of about 40 m, is solid sandstone and sandstone shale. Landslide movements occur periodically, mainly after heavy rainfall. The average annual flow rate of the landslide in the active parts of the landslide does not exceed 20 mm/year. The landslide is under constant monitoring by geologists and there are permanent inclinometer wells drilled on it.

For the selected borehole, studies of the magnetic component emission of the EM field were carried out with a prototype research apparatus. The research was carried out in the summer months of the year, during the dry season when the landslide does not manifest geodynamic activity. The magnetic field emission waveforms for the studied well are shown in Figure 11.

During the study, an underground magnetic field receiver was introduced to the maximum depth of the borehole, i.e. 30 m. The receiver was introduced three times by tuning it to different measurement frequencies of 7 kHz, 14 kHz and 19 kHz. For each frequency up to a depth of 3–4 m below the ground surface, increased field emission was observed. The recorded emission is related to the penetration of parasitic electromagnetic fields into the ground, interfering with the conducted measurements. From a depth of 4 m, the underground receiver reads the emission of

the magnetic component at a level of about A/m. The recorded field assumes a constant value for each of the applied frequencies along the entire measurement depth. Receiving such a low value of field strength at any depth, indicates the absence of active landslide movements.

However, the recorded low value of the field strength may indicate existing internal stresses in the landslide, causing a constant magnetic field emission.

Active landslide in Jarosow

The landslide in Jarosow has a homogeneous geological structure and is composed of a mixture of clay, sand and gravel. In the lower parts there are inclusions in the form of sandstone sheets of varying sizes. Based on many years of geological research including inclinometric measurements and analysis of the geomorphological structure, it is estimated that the landslide slippage occurs in deeper layers below 5 meters. When the landslide is active, the displacement reaches 40 mm/month.

Measurements of the magnetic component of the EM field were carried out on the landslide for an example inclinometer borehole. The measurements were made in the month of August abundant in precipitation. Magnetic field emission profiles for different measurement frequencies (7, 14, 19 kHz) are shown in Figure 12.

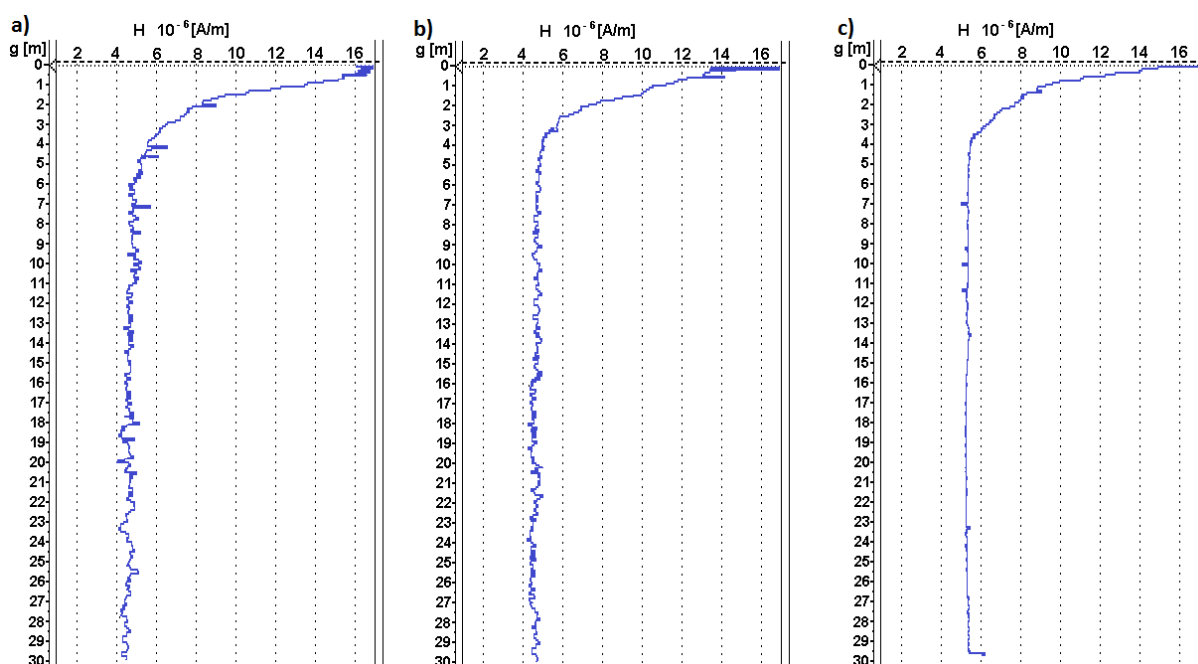


Fig. 11. Magnetic field intensity waveforms along the Leslaw borehole for the measurement frequency of the receiver (a) $f = 7$ kHz (b) $f = 14$ kHz (c) $f = 19$ kHz

As in previous measurements, to a depth of about 3-4m, the strong influence of electromagnetic disturbances penetrating below the ground surface is noticeable. For the studied landslide, anomalies in the recorded magnetic component are visible at depths of 7 to 8 meters and below 11m. This indicates increased activity of the landslide at the indicated depths. Presumably, the landslide manifests its activity at depths corresponding to increased hydration of the landslide layers. A sensitive method for detecting such situations is the electrical resistivity method with the help of which the resistivity of the geological layers of the subsoil is determined. With homogeneous geological structure of the studied layers, increased hydration corresponds to a lower value of resistivity. The probing depth of this method depends on the spacing of the measuring electrodes.

As a complement to the electromagnetic measurements, an electrofusion verification survey was conducted centrally over the surveyed borehole. Probing was carried out to a depth of 25 m using a ground electrode system in a Wenner configuration. The obtained resistivity measurement results are shown in Figure 13.

Analysis of the obtained sounding curve shows that up to a depth of about 2m the resistivity value is unchanged at about 25 Ωm. Which is due to the uniform moisture content of the near-surface soil layers. When further increasing the depth of penetration to 4–5 m, the resistivity increases, reaching a maximum value of 40 Ωm. Which indicates the low moisture content of these geological layers. From a depth of 6m, a gradual decrease in the resistivity value to a minimum value of 15 Ωm is observed. The reduced value

of resistivity at a uniform geological structure indicates increased hydration of the layer under consideration.

The apparent correlation of the results of the two methods testifies to the active movement of the landslide at depths below 7 m.

CONCLUSIONS

The designed and manufactured apparatus for measuring the electromagnetic activity of landslides offers new possibilities for assessing the stability of landslides. With this apparatus, it is possible to assess active movements in the landslide structure with an indication of existing slip planes in its body.

The measurement involves inserting an underground receiver of the magnetic component of the EM field into the test borehole and recording the field component at each depth of the borehole. Tests were conducted on two types of landslides: a periodically inactive one in Szymbark and an active one in Jaroszow. In both cases, up to a measurement depth of about 3-4m, an elevated level of magnetic field is recorded, associated with the penetration of electromagnetic disturbances associated with human infrastructure underground. During measurements of the inactive landslide, along the measurement well, magnetic field emission of low value is observed at a constant level. The recorded low value is probably related to the existing mechanical stresses keeping the landslide in equilibrium. The situation is different in the case of an active landslide in Jaroszow. Here, after the receiver is sunk below the depth of penetration of electromagnetic disturbances, a

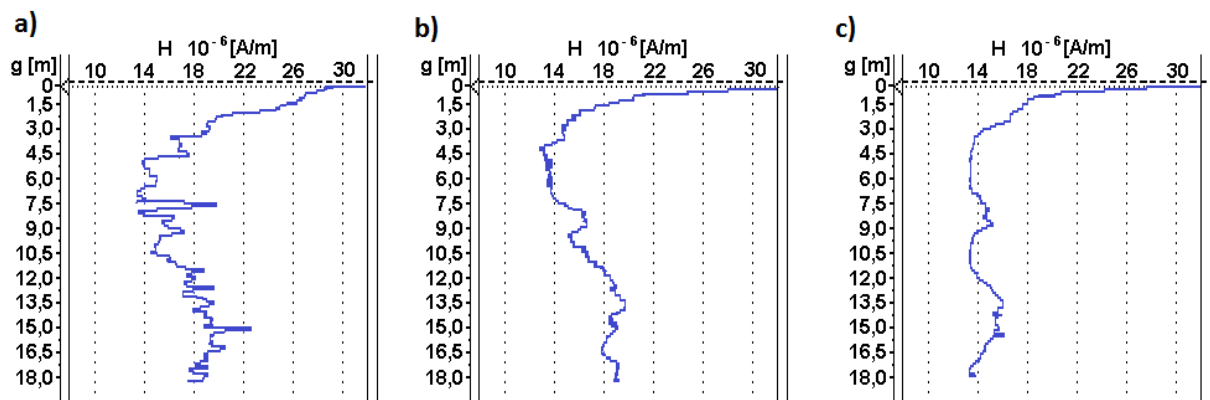


Fig. 12. Magnetic field intensity waveforms along the borehole in Jaroszow for the receiver measurement frequency: a) $f = 7$ kHz b) $f = 14$ kHz c) $f = 19$ kHz

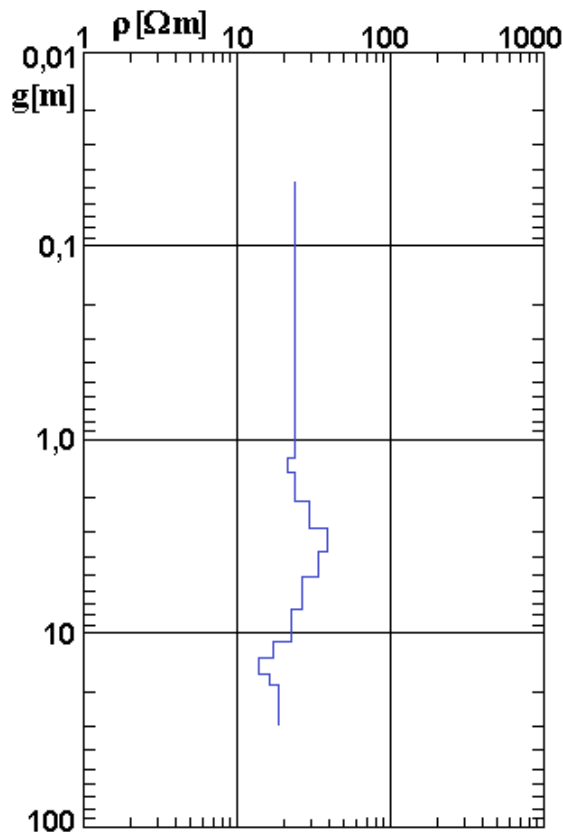


Fig. 13. Curve of electrical resistivity sounding along the borehole on the landslide in Jaroszow

renewed increase in recorded intensities is visible starting from 7 meters depth. This phenomenon is associated with the existence of slip zones in these parts of the landslide. A similar conclusion can be drawn by analyzing the profile of the electrical resistivity sounding conducted over the Jaroszow borehole. At depths corresponding to increased levels of magnetic field emissions, minimal resistivity values are observed, which may indicate hydration of the studied landslide layers.

The measurements carried out on actual landslides confirmed the effectiveness of the designed high-sensitivity measuring apparatus, indicating precisely the slip planes. An additional advantage of the apparatus is the possibility of continuous monitoring of landslide movements. This is possible by deploying a network of receivers in boreholes drilled in the body of the landslide at depths corresponding to potential slip planes. The recorded elevated emission value of the magnetic component of the EM field would indicate active landslide movement.

At the current stage of development of measurement apparatus, it is possible to use it as a method complementary to the commonly used systems for monitoring the status of landslide activity.

REFERENCES

- Petrucci O., Landslide Fatality Occurrence: A Systematic Review of Research Published between January 2010 and March 2022. *Sustainability* 2022; 14: 1-18.
- Urbański A., Grodecki M. Piles system securing road against landslide. 2D/3D method of numerical modeling and design problems. *Bulletin of the Polish Academy of Sciences Technical Sciences* 2020; 68: 1433-1442.
- Hungr O., Leroueil S. The Varnes classification of landslide types, an update. *Landslides* 2014; 11: 167-194.
- Argyriou A.V., Polykretis C., Teeuw C.R.M., Papadopoulos N. Geoinformatic Analysis of Rainfall-Triggered Landslides in Crete (Greece) Based on Spatial Detection and Hazard Mapping. *Sustainability* 2022; 14: 1–25.
- Stark T.D., Choi H. Slope inclinometers for landslides. *Landslides* 2008; 5: 339-350.
- Stumvoll M.J., Canli E., Engels A., Thiebes B., Groiss B., Glade T., Schweigl J., Bertagnoli M. The “Salcher” landslide observatory – experimental long-term monitoring in the Flysch Zone of Lower Austria. *Bulletin of Engineering Geology and the Environment* 2019; 79: 1-18.
- Jaboyedoff M., Carrea D., Derron M.H., Oppikofer T., Penna I.M., Rudaz B. A review of methods used to estimate initial landslide failure surface depths and volumes. *Engineering Geology* 2020; 262: 1-18
- Wang G.O. Millimeter-accuracy GPS landslide monitoring using Precise Point Positioning with Single Receiver Phase Ambiguity (PPP-SRPA) resolution: a case study in Puerto Rico. *Journal of Geodetic Science* 2013; 3: 22-31.
- Zhu X., Xu Q., Zhou J., Deng M. Remote landslide observation system with differential GPS. *Procedia Earth and Planetary Science* 2012; 5: 70-75.
- Saha A., Govind V., Villuri K., Bhardwaj A. Development and assessment of GIS-based landslide susceptibility mapping models using ANN, fuzzy-AHP, and MCDA in Darjeeling Himalayas West Bengal. *India. Land* 2022; 11: 1-27.
- Zainal M., Munir B., Marwan M. The electrical resistivity tomography technique for landslide characterization in Blangkejeren Aceh. *Journal of Physics: Conference Series IOP Publishing* 2021; 53: 1-14.
- Heinze T., Limbrock J.K., Pudasaini S.P., Kemna A. Relating mass movement with electrical self-potential signals. *Geophysical Journal International* 2018; 216: 55-60.
- Akinlabi I.A., Akinrimisi, O.E., Fabunmi M.A. Sub-surface investigation of landslide using electrical resistivity and self-potential methods in Oke-Igbo,

- Southwestern Nigeria. *IOSR Journal of Applied Geology and Geophysics* 2018; 6: 67-74.
14. Borecka A., Herzig J. Ground penetrating radar investigations of landslides: a case study in a landslide in Radziszów. *Studia Geotechnica et Mechanica* 2015; 37: 1-8.
 15. Moretto S., Bozzano F., Mazzanti P. The Role of Satellite InSAR for Landslide Forecasting: Limitations and Openings. *Remote Sensing* 2021; 13: 1-31.
 16. Huang C., Li F., Wei L., Hu X., Yang Y. Landslide susceptibility modeling using a deep random neural network. *Applied Sciences* 2022; 12: 1-19.
 17. Li H.W.M., Lo F.L.C., Wong T.K.C., Cheung R.W.M. Machine learning-powered rainfall-based landslide predictions in Hong Kong – An exploratory study. *Applied Sciences* 2022; 12: 1-24.
 18. Esmaeilabadi R., Shahri A.A. Prediction of site response spectrum under earthquake vibration using an optimized developed artificial neural network model. *Advances in Science and Technology Research Journal* 2016; 10(30): 76-83
 19. Hoffman M. On potential use of natural electromagnetic emissions in ELF, VLF and HF radio bands at active landslide areas: Preliminary results from Vinohrady nad Vahom site (Slovakia). *Contributions to Geophysics and Geodesy* 2022; 52: 113-125.
 20. Greiling R.O., Obermeyer H. Natural electromagnetic radiation (EMR) and its application in structural geology and neotectonics. *Journal Geological Society of India* 2010; 25: 278-288.
 21. Krumbholz M. Electromagnetic radiation as a tool to determine actual crustal stresses – applications and limitations. Doctoral thesis; Georg-August-Universität zu Göttingen; Germany, 2010
 22. Meng Y., Chen G., Huang M. Piezoelectric materials: properties, advancements, and design strategies for high-temperature applications. *Nanomaterials* 2022; 12: 1-32.
 23. Reppert P.M., Morgan F.D., Lesmes D.P., Jouniax L. Frequency dependent streaming potentials. *Journal of Colloid and Interface Sciences* 2001; 234: 194-203.
 24. Pride S.R., Morgan F.D. Electrokinetic dissipation induced by seismic waves. *Geophysics* 1991; 56: 902-1121.
 25. Adler P.M. Macroscopic electroosmotic coupling coefficient in random porous media. *Mathematical Geology* 2001; 33: 63-93.
 26. Eccles D., Sammonds P.R., Clint O.C. Laboratory studies of electrical potential during rock failure. *International Journal of Rock Mechanics & Mining Sciences* 2005; 42: 933-949.
 27. Heister K., Kleingeld P.J., Keijzer T.J.S., Loch G. A new laboratory set-up for measurement of electrical, hydraulic and osmotic fluxes in clays. *Engineering Geology* 2005; 77: 295-393.
 28. Kharkhalis N.R. Manifestation of natural electromagnetic pulse emission on landslide slopes. *Geophysical Journal* 1995; 14: 437-443.
 29. Fedorov E., Pilipenko V., Uyeda S. Electric and magnetic fields generated by electrokinetic processes in a conductive crust. *Physics and Chemistry of the Earth* 2001; 26: 793-799.
 30. Kormiltsev V.V., Ratushnyak A.N., Shapiro V.A. Three dimensional modeling of electric and magnetic fields induced by the fluid flow in porous media. *Physics of the Earth and Planetary Interiors* 1998; 105: 109-118.
 31. Lin P., Wei P., Wang C., Kang S., Wang X. Effect of rock mechanical properties on electromagnetic radiation mechanism of rock fracturing. *Journal of Rock Mechanics and Geotechnical Engineering* 2021; 13: 798-810.
 32. Tietze U., Schenk C., Gamm E. *Electronic Circuits Handbook for Design and Application*, 2nd ed.; Springer, 2011.
 33. Bolton T., Cohen M.B. Optimal design of electrically-small loop receiving antenna. *Progress In Electromagnetics Research C* 2020; 98: 155–169.
 34. Dyo V., Ajmal T., Allen B., Jazani D., Ivanov I. Design of a ferrite rod antenna for harvesting energy from medium wave broadcast signals. *The Journal of Engineering* 2013; 12: 89-96